AGU PUBLICATIONS

JGR

Journal of Geophysical Research: Solid Earth

RESEARCH ARTICLE
10.1002/2015JB012584

Key Points:
- Faulting types of small earthquakes are classified based on waveform similarity
- Interplate seismicity shows locked and slipping areas after the M9 earthquake
- Faulting type distribution is consistent with the stress due to the main shock

Supporting Information:
- Supporting Information S1
- Data Set S1

Correspondence to:
W. Nakamura,
w_nakamura@met.kishou.go.jp

Citation:
Nakamura, W., N. Uchida, and T. Matsuzawa (2016), Spatial distribution of the faulting types of small earthquakes around the 2011 Tohoku-oki earthquake: A comprehensive search using template events, *J. Geophys. Res. Solid Earth*, *121*, doi:10.1002/2015JB012584.

Received 8 OCT 2015
Accepted 18 MAR 2016
Accepted article online 25 MAR 2016

Spatial distribution of the faulting types of small earthquakes around the 2011 Tohoku-oki earthquake: A comprehensive search using template events

Wataru Nakamura[1,2], Naoki Uchida[1], and Toru Matsuzawa[1]

[1]Research Center for Prediction of Earthquakes and Volcanic Eruptions, Graduate School of Science, Tohoku University, Sendai, Japan, [2]Now at Japan Meteorological Agency, Chiyoda, Japan

Abstract We developed a new method to classify the faulting types of small earthquakes using interevent waveform similarity and applied it to earthquakes in the northeast Japan subduction zone. In the method, we used separate time windows for *P* and *S* waves and established a relationship between waveform similarity and differences in focal mechanisms from event pairs whose focal mechanisms we know. Then we applied the relationship to many pairs of such focal-mechanism-known events (5607 from the moment tensor catalogue and 3623 events from the interplate repeating earthquakes catalogue) and focal-mechanism-unknown events for the period from 1984 to 2013. As a result, 8984 earthquakes were newly classified into interplate ($N = 5401$), noninterplate thrust ($N = 631$), normal ($N = 1070$), and strike-slip faulting earthquakes ($N = 165$). From the new data set, which doubles the number of mechanism types, we confirmed that there have been almost no interplate earthquakes in the area of large coseismic slip of the Tohoku-oki earthquake since that event. We also saw that this trend continued until at least the end of 2013, suggesting a nearly complete stress release and slow interplate stress recovery. The abundant interplate aftershocks also indicate the precise spatial extent of postsesimic slip, which is usually difficult to obtain from land-based geodetic data. The postseismic slip also suggests stress concentration at the asperities of the 1968 Tokachi-oki (*M*7.9) and 1994 Sanriku-oki (*M*7.6) earthquakes. The present-day faulting types offshore Tohoku correlated well with the static-stress change from the Tohoku-oki earthquake, suggesting a stress state change during the earthquake cycle of megathrust earthquakes.

1. Introduction

On 11 March 2011 14:46 (JST), the great Tohoku-oki earthquake (M_w9.0) struck northeastern Japan. A number of studies using seismic waveform data, onshore and offshore geodetic data, or tsunami waveform data [e.g., *Ide et al*., 2011; *Iinuma et al*., 2012; *Satake et al*., 2013] have revealed an area with concentrated large coseismic slip near the Japan trench, off Miyagi Prefecture and the vast source area along the Japan trench.

The Tohoku-oki earthquake brought stress changes and consequent seismicity changes in and around the source region [e.g., *Toda et al*., 2011; *Hasegawa et al*., 2011; *Okada et al*., 2011]. For example, in the area that underwent large coseismic slip during the 2011 Tohoku-oki earthquake, the number of interplate and repeating earthquakes has been reported as having dramatically decreased after the *M*9 earthquake [e.g., *Asano et al*., 2011; *Kato and Igarashi*, 2012; *Uchida and Matsuzawa*, 2013]. At the same time a large number of normal faulting earthquakes has occurred in the same area [e.g., *Asano et al*., 2011; *Obana et al*., 2012; *Hardebeck*, 2012]. To gain a deep understanding of the Tohoku-oki earthquake and to improve practical earthquake hazard estimation in the subduction zone, it is important to know how the seismicity around the source area is characterized and how it changed after the great earthquake.

Focal-mechanism information reveals earthquakes' faulting style and is useful in interpreting earthquake generating stress and tectonics [e.g., *Ito et al*., 2004; *Asano et al*., 2011]. In general, focal mechanisms are evaluated using moment tensor (MT) solutions or *P* wave first motions, but it is difficult to estimate them for small offshore earthquakes due to insufficient station coverage and/or the waveform data's poor signal-to-noise ratios.

Template events or waveform similarity is often used to detect unknown events [e.g., *Peng and Zhao*, 2009; *Kato et al*., 2012; *Kato and Nakagawa*, 2014] and repeating earthquakes [e.g., *Poupinet et al*., 1984; *Uchida and Matsuzawa*, 2013]. Waveform similarity assures small interevent distances and similar focal mechanisms

[*Menke et al*., 1990; *Menke*, 1999; *Nakahara*, 2004]. In this study, we developed a new method that evaluates waveform similarity to classify the faulting types of small offshore earthquakes whose focal mechanisms are unknown based on conventional methods. We examined the empirical relationship between the degree of difference in focal mechanisms and waveform cross-correlation coefficients of earthquake pairs with known focal mechanisms. In the relationship, we determined a threshold of cross-correlation coefficient above which we can consider them to have similar mechanisms. Then based on the cross-correlation threshold, we classified the faulting types of events with unknown focal mechanisms, using those with known mechanisms as templates. Using the results of the classification, we discuss the spatial distribution of faulting types before and after the 2011 Tohoku-oki earthquake. This discussion takes the earthquakes' relocated hypocenters into account using the double-difference tomography method [*Zhang and Thurber*, 2003, 2006] based on a simple 3-D velocity structure. We also examine the spatial distribution of postseismic slip and off-fault seismicity based on the focal mechanisms and coseismic stress changes.

2. Relationship Between Focal Mechanism Difference and Waveform Similarity

At a station where the recording system has not changed, seismograms recorded depend on source processes, ray paths, medium changes, and time-dependent noises. An example of earthquakes that exhibit nearly identical waveforms is a group of repeating earthquakes that occur at the same patch on a fault [e.g., *Ellsworth*, 1995; *Uchida and Matsuzawa*, 2013]. Their focal mechanisms and locations are almost identical. Waveform correlation can be used to ensure that the sources have the same focal mechanism even if they are slightly separated or space [e.g., *Menke et al*., 1990; *Nakahara*, 2004].

To evaluate the relationship between focal mechanism differences and waveform similarities, we used F-net (Broadband Seismograph Network) focal mechanism data. The F-net focal mechanisms are determined by the National Research Institute for Earth Science and Disaster Prevention (NIED) using broadband seismograph data and a moment tensor inversion method [*Dreger and Helmberger*, 1993; *Fukuyama et al*., 1998]. To ensure the quality of the mechanism solutions, we selected 5608 focal mechanisms whose variance reductions are larger than 0.8 to use as earthquakes with known focal mechanisms (Figure 1a); the validity of using 0.8 as the selection criteria was confirmed using repeating earthquake data. For the waveform data to evaluate waveform similarities, the seismograms from the seismic network of Hokkaido University, Hirosaki University, Tohoku University, and the University of Tokyo were used (Figure 1a). This station distribution of these seismic networks are sparse compared to the High-Sensitivity Seismograph Network (Hi-net), but digital waveform data from these networks are available for the longer time period (from 1984) than Hi-net. The seismic network are mostly consist of short period (1 Hz) seismometers and sampled at 100 Hz. Most of the seismic stations are located in vaults or boreholes. For the evaluation of the relationship between focal mechanism differences and waveform similarities, we analyzed the period from 2002 to 2013 which is the period F-net focal mechanisms are available. No waveform data were available at some stations for 2–14 days after the occurrence of the Tohoku-oki earthquake due to electric power and data transmission problems caused by the earthquake.

The similarity of the waveforms and focal mechanisms of two events are quantified, respectively, by their cross-correlation coefficient (CC) and the minimum 3-D rotation angle (hereafter "Kagan's angle") [*Kagan*, 1991] between them. We calculated CC values for *P* and *S* waves separately to reduce the effect of differences in *S-P* times. The optimal window lengths were determined so as to maximize the number of new mechanism types detected and to minimize misidentification. This will be described in the last part of this section in detail. When we calculated the CCs, we used waveforms in as low a frequency band as possible because lower frequency waveforms are less affected by interevent distances, [e.g., *Menke et al*., 1990; *Menke*, 1999; *Nakahara*, 2004] but are still sensitive to differences in focal mechanism. We adopted 0.1–2.0 Hz band-pass filters for the waveforms. However, low-frequency waveform sometimes does not have enough amplitude compared to microseisms for small earthquakes whose mechanism type we are intending to classify. Therefore, when the signal-to-noise ratio (SNR) of the frequency band was less than 2.0, we adopted 1.0–4.0 Hz, 2.0–8.0 Hz, and 4.0–16.0 Hz band-pass filters for waveforms one after another until the SNR exceeded 2.0. In the calculation, SNR is defined as the amplitude ratio between the waveform in a range from 1.0 s before to 2.0 s after the *P* wave onset (signal) and the waveform in a range from 6.0 s to 2.0 s before the

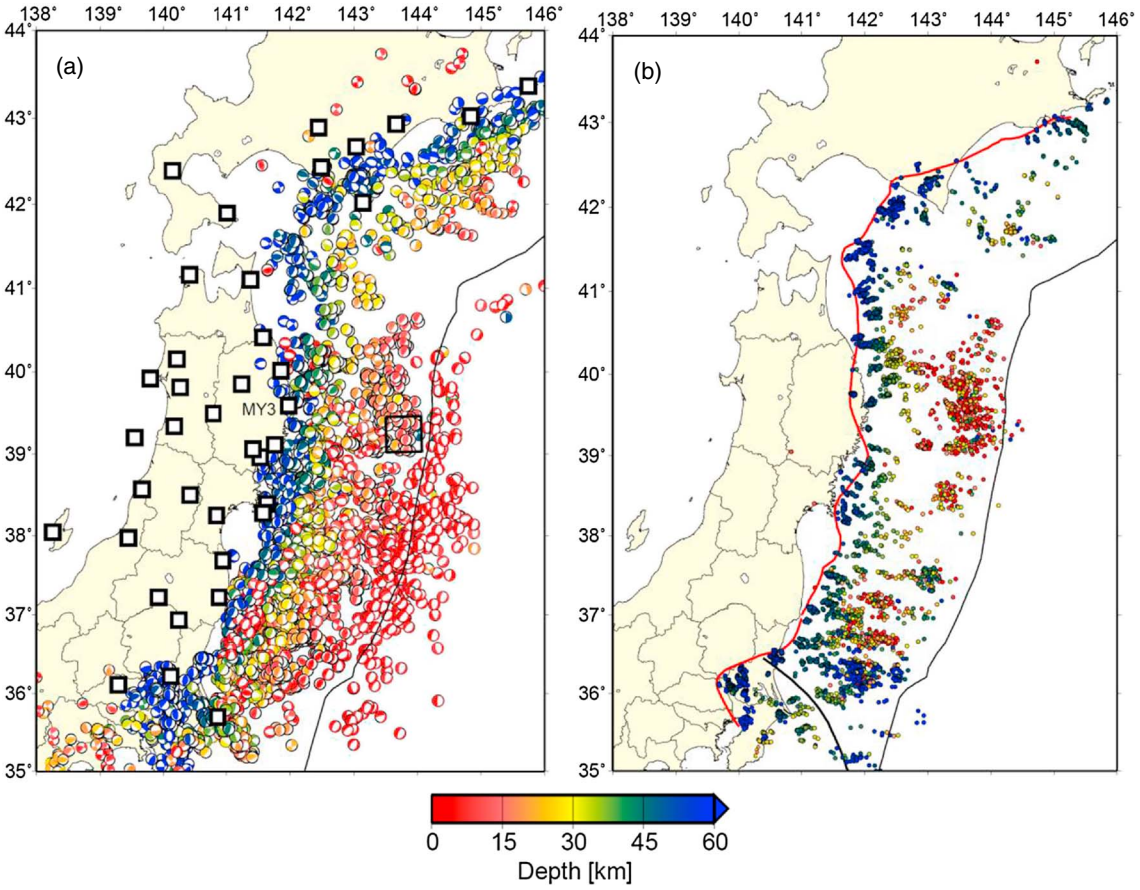

Figure 1. Distribution of earthquakes that are used as initial template events. (a) Focal mechanisms of earthquakes in the northeastern Japan subduction zone from October 1997 to December 2013 reported in the F-net catalogue. Color indicates the focal depth of the earthquake. White squares delineated by black lines are seismic stations used for the calculations of the waveform cross correlation that are operated by Hokkaido University, Hirosaki University, Tohoku University, and the University of Tokyo. Waveforms of some events located in the offshore black square are shown in Figure 2. (b) Locations of repeating earthquakes detected by *Uchida and Matsuzawa* [2013]. Color indicates focal depth. The red line indicates the downdip limit of interplate earthquakes [*Igarashi et al*., 2001; *Kita et al*., 2010; *Uchida et al*., 2009]. Black lines represent the Japan trench and northeast limit of the subducted Philippine Sea Plate [*Uchida et al*., 2009].

onset (noise). If the SNR for a 4.0–16.0 Hz filtered waveform was less than 2.0, it was no longer used in the later analysis. In the final result described in section 4, the percentage of used frequency band are 58.1, 31.1, 8.0 and 2.8% for 0.1–2.0 Hz, 1.0–4.0 Hz, 2.0–8.0 Hz, and 4.0–16.0 Hz, respectively. The specific cross-correlation coefficient (CC) of an event pair is defined as the average of cross-correlation coefficients for *P* waves (CCp) and *S* waves (CCs):

$$CC = (CCp + CCs)/2.$$

The CCp comes from the vertical component seismograms while the CCs is evaluated by averaging the cross-correlation coefficients of the two orthogonal horizontal components. We finally averaged CC for 10 stations from highest CC value. If the number of available stations are less than three, the event pair was not used for the later analysis.

Examples of waveforms of earthquakes located in the open square observed at station MY3 (Figure 1a) are shown in Figure 2. The first waveform is the reference event that occurred on 19 October 2006. In this case, the third and ninth waveforms are similar ($CC >= 0.64$) to the first waveform and their focal mechanisms are also similar (Kagan's angle < 30). On the other hands, the eighth waveform, for the event on 12 November 2010 is apparently different from the first one and the focal mechanisms of the two events are not similar. The other events' waveform similarities and Kagan's angles are between these two extremes.

Figure 3a shows an example of the relationship among CC, interevent distance, and Kagan's angles for 792 earthquakes that occurred off Miyagi (Figure 3c) from 2002 to 2013. We found that event pairs with large

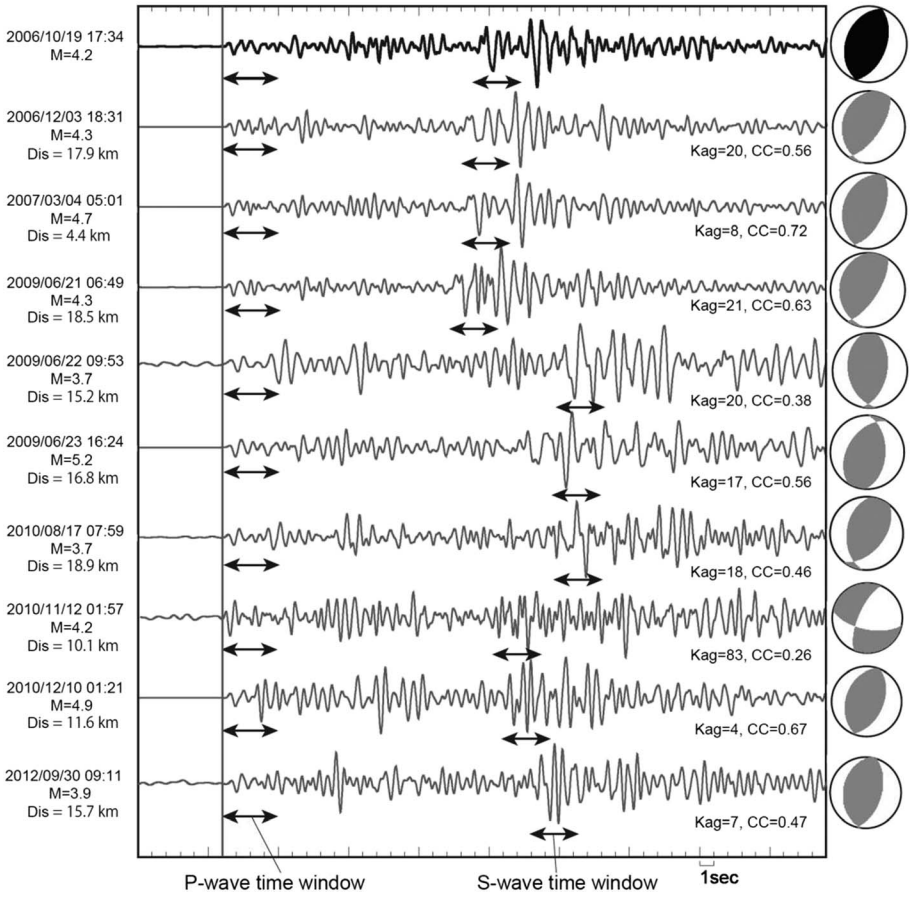

Figure 2. Examples of waveforms and focal mechanisms of earthquakes that occurred in the area indicated by black square in Figure 1a. The waveform is up-down component observed at station MY3 (Figure 1a). The first event (top waveform in the figure) is the reference event for calculating CC values. Black bidirectional arrows indicate 4.0 and 3.5 s time windows for calculation of CC values for *P* and *S* waves, respectively. Waveforms are filtered at a pass band of 0.1–2.0 Hz. Origin time, magnitude, and horizontal distance from the reference event are labeled to the left of the waveforms and F-net focal mechanisms, Kagan angles, and CC values are shown to the right.

CC values always have small Kagan's angles and small interevent distances (Figure 3a). We set CC value thresholds for several regions including the off-Miyagi area in order to select earthquakes with similar focal mechanisms. To determine the proper CC threshold, we used event pairs whose Kagan's angles were smaller than 30°. In Figure 3a, N1 represents the number of event pairs (Group 1) whose cross-correlation coefficients are larger than a given CC value (CC_0) as indicated by the gray box; N2 shows the number of event pairs (Group 2) whose Kagan's angles are smaller than 30° and whose cross-correlation coefficients are larger than CC_0. Note that Group 2 is a subset of Group 1. We then increased the CC_0 value by 0.01 increments from 0.00 to 1.00 and selected the CC_0 threshold where the ratio of N2 to N1 first exceeded 0.9. This means if an event pair has a CC larger than the threshold, there is a 90% probability that its Kagan's angle is 30° or smaller.

In order to obtain as many classified events as possible, we searched for *P* and *S* wave time window lengths that maximize the number of pairs in N2 (Figure 3b) using the events located off Miyagi Prefecture. From a grid search from 1.0 s to 5.0 s, we found that a time window of 4.0 s is best for *P* waves and 3.5 s is best for *S* waves for events offshore Miyagi (Figure 3b). The CC threshold for the best time windows is 0.65. N2 tends to be larger with longer time windows (Figure 3b), but to avoid contaminating the *P* wave time window with *S* waves, we searched for the best time window length shorter than 5 s. We sought and determined thresholds for other regions using the same procedure. The resulting thresholds range from 0.60 to 0.66 (Figure 3c).

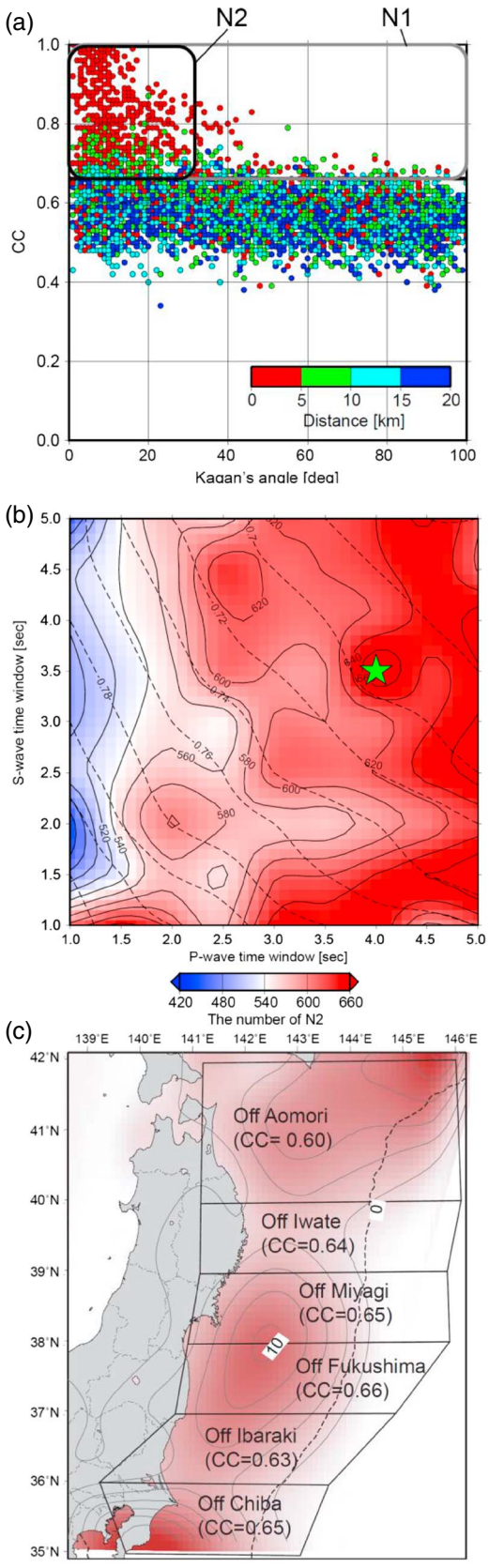

3. Classification of Small Earthquakes' Faulting Types

By using the CC threshold determined in the previous section, we classified earthquakes with magnitude 3 or larger in the NE Japan subduction zone (Figure 1) into several faulting type groups. The waveform data are from the same seismic networks as for the CC threshold determination (Figure 1a), but longer time period (from July 1984 to December 2013) are used for the classification. We used 5607 events with known focal mechanisms from the F-net data spanning 1997 to December 2013 (Figure 1a) and 3623 repeating earthquake from July 1984 to December 2011 (Figure 1b) [*Uchida and Matsuzawa*, 2013] as template events. We interpret repeating earthquakes as representing repeated slips of patches or asperities on plate boundary faults. The magnitude of repeating earthquakes are $M \geq 2.5$ and $M \geq 4.0$ for the period before and after the 2011 Tohoku-oki earthquake, respectively.

We calculated CC values for every pair of events that were separated by less than 20 km horizontally, and where the faulting type of one event (template event) was known but the other (target event) was not. First, we found 7723 events that had CC values larger than the threshold when paired with events with known mechanisms. We then used these 7723 events as new template events and iterated the process until no new event pairs had CC values exceeding the threshold. In this way we were able to newly classify a total of 8984 events. The process usually finished within four iterations. This iterative process may accumulate focal-mechanism difference from the original template and does not guarantee that the selected event has Kagan's angle smaller than 30° with 90% probability. However, we confirmed that this effect is small and the newly classified events have focal mechanisms that are similar to their respective initial template events (see supporting information).

Figure 3. Procedure for determining parameters to classify faulting types from waveform similarities. (a) Relationship between Kagan's angle and CC for event pairs off Miyagi (Figure 3c). Color indicates the interevent horizontal distance of each earthquake pair. N1 is the number of pairs (Group 1) whose CCs are larger than value CC_0, and N2 is the number of pairs (Group 2) that belong to Group 1 and whose Kagan's angles are less than 30°. (b) Dependence of N2 on the *P* and *S* wave time window lengths. Color and solid contours indicate the N2 value calculated from the time window lengths for *P* waves (abscissa) and *S* waves (ordinate). Dashed contours indicate CC thresholds for each time window set. (c) CC thresholds for respective regions for the time window of 4.0 s (*P* wave) and 3.5 s (*S* wave). Color and contour represent the slip deficit on the plate boundary before the Tohoku-oki earthquake [*Suwa et al.*, 2006].

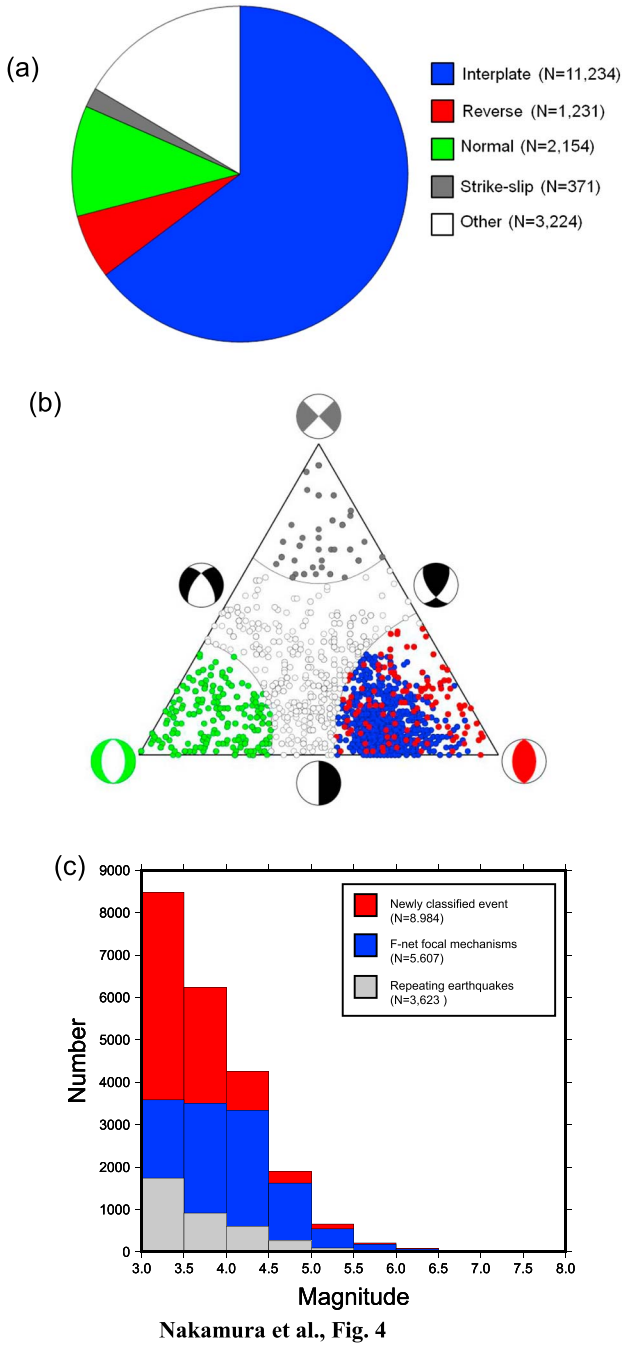

Figure 4. Characteristics of faulting types obtained in this study. (a) Pie chart for all the faulting-type data (original templates and newly classified events). (b) Triangle diagram [*Frohlich*, 1992] for earthquakes used in this study. Symbol color is the same as in Figure 4a. (c) Frequency distribution of earthquake magnitude for original templates and newly classified events. Gray and blue areas, respectively, indicate repeating earthquakes and earthquakes with F-net focal mechanisms used as template events in this study. Red area indicates the earthquakes that are newly classified into several faulting types in this study.

We classified the newly obtained events into normal, thrust, strike-slip, and other faulting types based on the triangle diagram introduced by *Frohlich* [1992]. The following criteria were thus adopted when classifying the faulting types.

$$\begin{aligned} \text{Thrust faulting type:} &\quad \sin^2\delta T > 0.59 \\ \text{Normal faulting type:} &\quad \sin^2\delta P > 0.75 \\ \text{Strike-slip faulting type:} &\quad \sin^2\delta B > 0.75 \end{aligned}$$

Here, $\delta T, \delta P$, and δB are the plunges of the *T* axis, *P* axis, and *B* axis of the earthquake, respectively. We classified thrust faulting-type events into interplate and noninterplate events by comparing their focal mechanisms with theoretical focal mechanisms on the plate boundary. For this classification we used a simple method that if the following value (d*M*) is greater than 0.75, we regard the target event as an interplate-type earthquake [*Abers and Gephart*, 2001; *Kato and Igarashi*, 2012].

$$\mathrm{d}M = 0.5\left\{\left(\mathbf{p}^1\cdot\mathbf{p}^2\right)^2 + \left(\mathbf{t}^1\cdot\mathbf{t}^2\right)^2 - \left(\mathbf{p}^1\cdot\mathbf{t}^2\right)^2 - \left(\mathbf{p}^2\cdot\mathbf{t}^1\right)^2\right\}$$

Here $\mathbf{p}^1$ and $\mathbf{t}^1$ are the vectors of the *P* and *T* axes of theoretical focal mechanisms, and $\mathbf{p}^2$ and $\mathbf{t}^2$ are ones of the target event. Note that if the in situ depth of the plate boundary is shallower than 20 km, we applied a threshold of $\mathrm{d}M > 0.50$ due to insufficient constraint on the dip angle of focal mechanisms in the area.

The theoretical interplate-type focal mechanism was calculated by taking the spatial variation in the relative plate motion [*Sella et al.*, 2002] and plate geometry into account [*Nakajima and Hasegawa*, 2006; *Uchida et al.*, 2010; *Kita et al.*, 2010] at a 0.05° grid spacing on the plate boundary. Of the 8984 new events, this process resulted in classifying 6032 as thrust faulting, 1070 as normal faulting, 165 as strike-slip faulting, and 1717 as other faulting-type events as shown in Figure 4. Most of the events belonging to the thrust faulting type (91.7%) were interplate-type earthquakes. The magnitudes of newly identified events (shown in red in Figure 4c) range mostly from *M*3.0 to *M*4.0. In that range, there were only small numbers of faulting-type data in the original catalogue (Figure 4c). Faulting-type earthquakes (original template events and newly detected

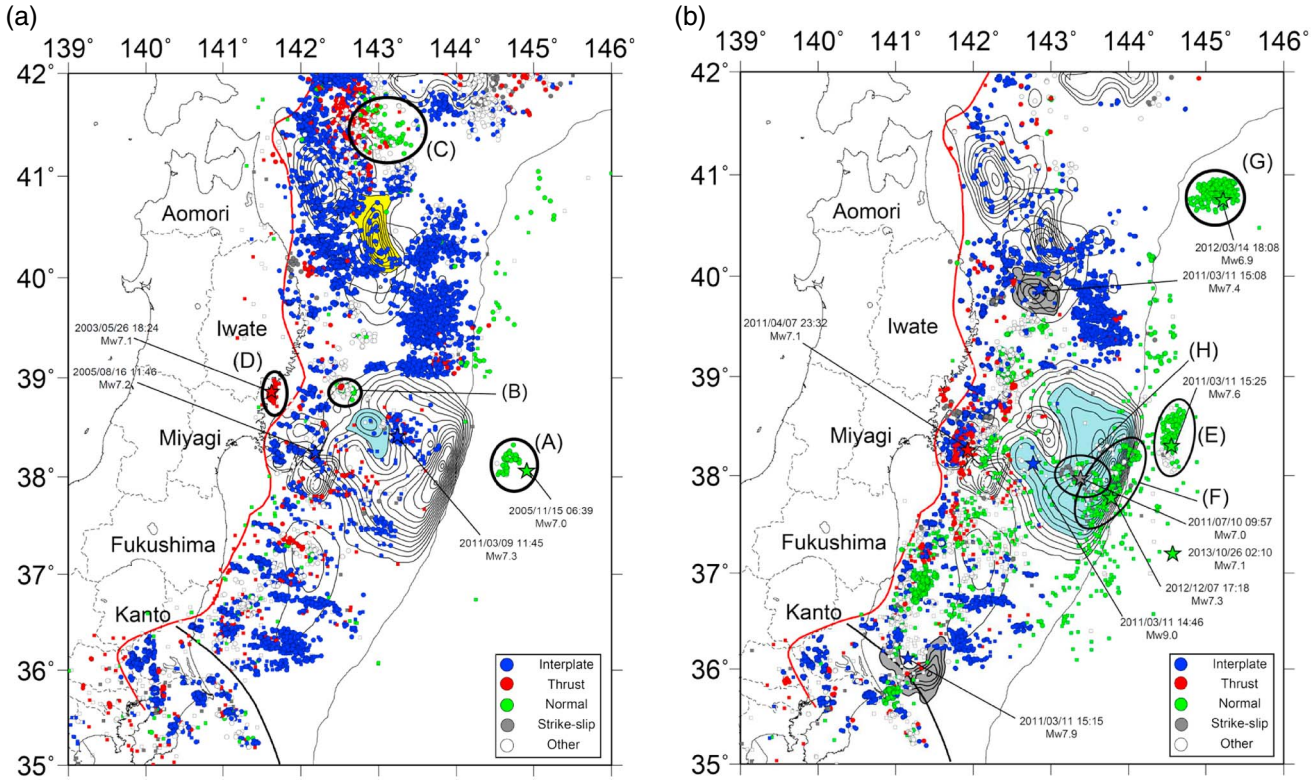

Figure 5. Spatial distributions of event faulting types (a) before (July 1984 to 11 March 2011, 14:45) and (b) after (11 March 2011, 14:46 to December 2013) the Tohoku-oki earthquake. Squares and circles indicate original template events (F-net focal mechanisms and repeating earthquakes) and events newly classified in this study, respectively. Blue, red, green, gray, and white symbols indicate interplate, noninterplate thrust faulting, normal faulting, strike-slip faulting, and other faulting-type events, respectively. Contours show slip distributions of major interplate events [*Yamanaka and Kikuchi*, 2003, 2004; *Iinuma et al*., 2012; *Ohta et al*., 2012]. Red and black lines are the same as those in Figure 1b. In Figure 5a, main source areas for the 1994 Sanriku-oki earthquake (*M*7.6) and the largest foreshock (*M*7.3) of the Tohoku-oki earthquake are shown by yellow and light blue areas, respectively. Black ellipsoids (regions (A)–(D)) indicate earthquake clusters including aftershock areas of the 2003 *M*7.1 (D) and 2005 *M*7.2 (A) intraplate earthquakes. In Figure 5b, the area with coseismic slip of ≥30 m from the Tohoku-oki earthquake [*Iinuma et al*., 2012] is light blue. The slip areas for two large aftershocks on 11 March 2011 (*M*7.4, *M*7.7) are shown by gray-filled contours [*Kubo et al*., 2013; *Muto et al*., 2014]. Black ellipsoids (regions (E)–(H)) indicate earthquake clusters including aftershocks of the major intraplate earthquakes that occurred at 15:25 JST, 11 March 2011 (*M*7.5), on 14 March (*M*6.9), and 7 December (*M*7.3) 2012. Stars indicate epicenters of major earthquakes.

events, $N = 18{,}214$) make up 25% of those studied here ($M \geq 3.0$). The origin time, location, and magnitudes of each faulting types are listed in the supporting information.

4. Results

4.1. Faulting-Type Distribution Before the Tohoku-Oki Earthquake

Figure 5a shows the spatial distribution of earthquakes whose faulting types are classified in this study (circles) and original template F-net data and repeating earthquakes (squares) for the period from July 1984 to 11 March 2011, 14:45 JST (just before the 2011 Tohoku-oki earthquake).

The distribution shows relatively sparse interplate events off Miyagi and Fukushima prefectures. In that area, a large slip deficit (strong interplate coupling) was estimated using geodetic data before the Tohoku-oki earthquake (Figure 3c) [e.g., *Suwa et al*., 2006; *Loveless and Meade*, 2010]. Comparing this distribution with the slip areas of $M > 7$ interplate earthquakes since 1930, including the 1968 *M*7.9, the 1994 *M*7.6 (yellow area) [*Nagai et al*., 2001; *Yamanaka and Kikuchi*, 2004], the *M*7.3 foreshock of the Tohoku-oki earthquake (light blue area) [*Ohta et al*., 2012], and the Tohoku-oki earthquake [*Iinuma et al*., 2012], shows that most of the small interplate earthquakes classified in this study are located outside of the main slip areas (Figure 5a). Low interplate seismicity in the area of large coseismic slip of the Tohoku-oki earthquake is particularly noticeable. In the zone of minor coseismic slip (outside the main slip areas of the $M > 7$ earthquakes), however, small interplate earthquakes do occur.

The noninterplate thrust faulting events (red squares and circles) are sparsely distributed, except for the cluster indicated by an ellipsoid (region (D) in Figure 5a) near the Miyagi coastline, most of which are aftershocks of an intraplate event (*M*7.1) that occurred in the subducting slab on 26 May 2003 (red star in Figure 5a).

Normal faulting events (green squares and circles) are also sparse, but there are some event clusters (regions (A)–(C) in Figure 5a). Most of the events in the outer trench ellipsoid (region (A) in Figure 5a) are aftershocks of a large normal faulting event (*M*7.2) on 15 November 2005 (green star in Figure 5a). The clustering of events in region (B) is also prominent, but there are no earthquakes whose magnitudes are larger than 6.0 in the period from 1984 to 2011. There have been no significant earthquakes in this area since the beginning of the JMA's catalogue (1923). Most of the events far off the east coast of Aomori Prefecture (region (C) in Figure 5a) were distributed relatively sparsely. In this region, the largest aftershock (*M*7.5) of the 1968 Tokachi-oki earthquake (*M*7.9) was a normal-faulting-type event [*Nakajima*, 1974]. Thus, these normal faulting events may indicate long-lasting aftershock activities more than two decades after the occurrence of the *M*7.5 large normal faulting event, or they may indicate some stress heterogeneity in the region related to plate bending at the Hokkaido corner. Strike-slip faulting events (gray squares and circles) rarely occurred in this period.

4.2. Faulting Type Distribution After the 2011 Tohoku-Oki Earthquake

Figure 5b shows the spatial distribution of faulting types from 11 March 2011, 14:46 JST to 31 December 2013 (after the Tohoku-oki earthquake). It shows nearly no interplate earthquakes (blue squares and circles) in the area that underwent large coseismic slip during the Tohoku-oki earthquake (light blue area in Figure 5b, slip $\geq$ 30 m), while there are many interplate earthquakes in surrounding areas. Interplate earthquakes are also inactive near the source of two large interplate aftershocks (*M*7.4, *M*7.6) on 11 March 2011 (blue stars and dark gray area in Figure 5b).

There is more normal faulting activity after the Tohoku-oki earthquake (green) than in the period before it throughout the study area (Figure 5). This implies that a tensional stress field has dominated after the earthquake. The normal faulting events have mainly occurred to the west of the Tohoku-oki earthquake's coseismic slip area (contour off Iwate to Kanto, 36–39.5° N) and near the Japan Trench (thin black line). The prominent normal faulting earthquake clusters near the Japan and Kuril trenches include large normal faulting events (green stars) at 15:25, 11 March 2011 (*M*7.5) in region E, on 14 March 2012 (*M*6.9) in region G and 7 December 2012 (*M*7.3) in region F.

Thrust faulting events (red) mainly occurred to the west of the Tohoku-oki earthquake's slip area (Figure 5b). They include a large thrust intraplate event on 7 April 2011 (*M*7.1) (red star in Figure 5b) and its aftershocks. An event on 7 December 2012 (*M*7.3) that occurred near the Japan Trench (green star in Figure 5b) is considered to be a doublet or composed of multiple intraplate events occurring within a few seconds: i.e., a deeper thrust faulting event followed by a shallower normal faulting event [e.g., *Harada et al*., 2013; *Lay et al*., 2013]. However, we could not find any deeper thrust faulting earthquakes in that region in this study, probably due to the lack of thrust faulting template events in the F-net catalogue there.

Strike-slip faulting events (gray) occur sparsely in and around the Tohoku-oki earthquake area, but small clusters of strike-slip faulting events are located east of its hypocenter (region H) where an *M*7.3 strike-slip earthquake occurred on 10 July 2011 (Figure 5b).

It is already discussed that stress state after the Tohoku-oki earthquake was significantly changed after the Tohoku-oki earthquake from the moment tensor solutions [e.g., *Asano et al*., 2011] and stress tensor inversion [e.g., *Hasegawa et al*., 2011]. Our result shows the clear change in mechanism type distribution from very large number of faulting type data.

4.3. Hypocenter Relocation in the 2011 Tohoku-Oki Earthquake Rupture Area

Precise locations of earthquake hypocenters are important when discussing the faulting type distribution of off-fault earthquakes. However, the locations of small offshore earthquakes, especially their depths, which are estimated from local on-land station data, sometimes have systematic errors due to insufficient azimuthal station coverage and the difference between actual and modeled velocity structures. To obtain better locations, we relocated the hypocenters using the double-difference tomography method

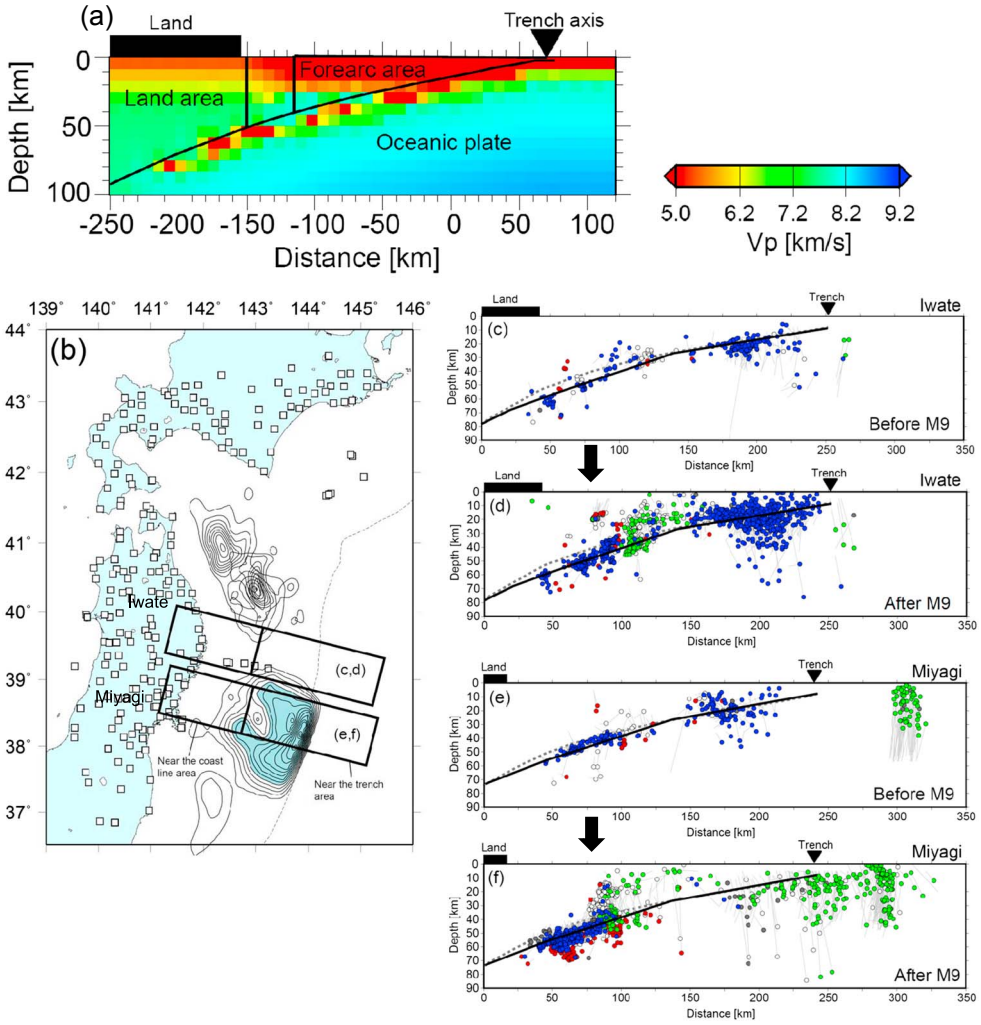

Figure 6. Earthquake relocation and depth distribution of earthquakes. (a) *P* wave velocity model across trench perpendicular cross section showing regions with different velocity structures. The land and forearc areas are determined by the depth of the plate boundary. (b) Distribution of seismic stations used to relocate hypocenters. Contours are the coseismic slip distribution of the Tohoku-oki earthquake [*Iinuma et al.*, 2012], 1968 Tokachi-oki and 1994 Sanriku-oki earthquakes [*Nagai et al.*, 2001; *Yamanaka and Kikuchi*, 2004]. Cross section off (c) Iwate and (d) Iwate and (e) Miyagi prefectures before the Tohoku-oki earthquake (rectangular regions in Figure 6b). Cross section off (f) Miyagi prefectures after the Tohoku-oki earthquake (rectangular regions in Figure 6b). Colors in Figures 6c–6f indicate faulting types in the same manner as in Figure 5. The gray lines connect the initial hypocenters (no symbol) and relocated hypocenters (colored circles). Black line and gray dashed line in Figures 6c–6f indicate plate boundary estimated in this study and by *Nakajima and Hasegawa* [2006], respectively.

[*Zhang and Thurber*, 2003, 2006] and a 3-D velocity structure for earthquakes located near the source area of the Tohoku-oki earthquake. Here we only estimated hypocenter locations and did not change the velocity structure in the inversion. The heterogeneous velocity structure offshore was taken into account by a simple 3-D velocity structure. The velocity structure is based on previous studies of land areas [*Hasegawa et al.*, 1978], forearc areas [*Hino et al.*, 2000], and oceanic plates [*Hino et al.*, 2009; *Shiina et al.*, 2013]. The land and forearc areas are defined by their range of plate boundary depths (10–40 km for forearc areas and 50 km or larger for land as shown in Figure 6a [*Nakajima and Hasegawa*, 2006; *Kita et al.*, 2010]). The portion between these areas is linearly interpolated. We used 216 seismic stations located in the Tohoku and Hokkaido regions (Figure 6b), and 1,703,365 *P* and 1,337,326 *S* wave arrival time data integrated by the Japan Meteorological Agency.

Cross sections (depth distribution) of faulting types across the large coseismic slip area off Miyagi Prefecture and north of the large coseismic slip area off Iwate Prefecture (rectangular areas, Figure 6b) show that normal

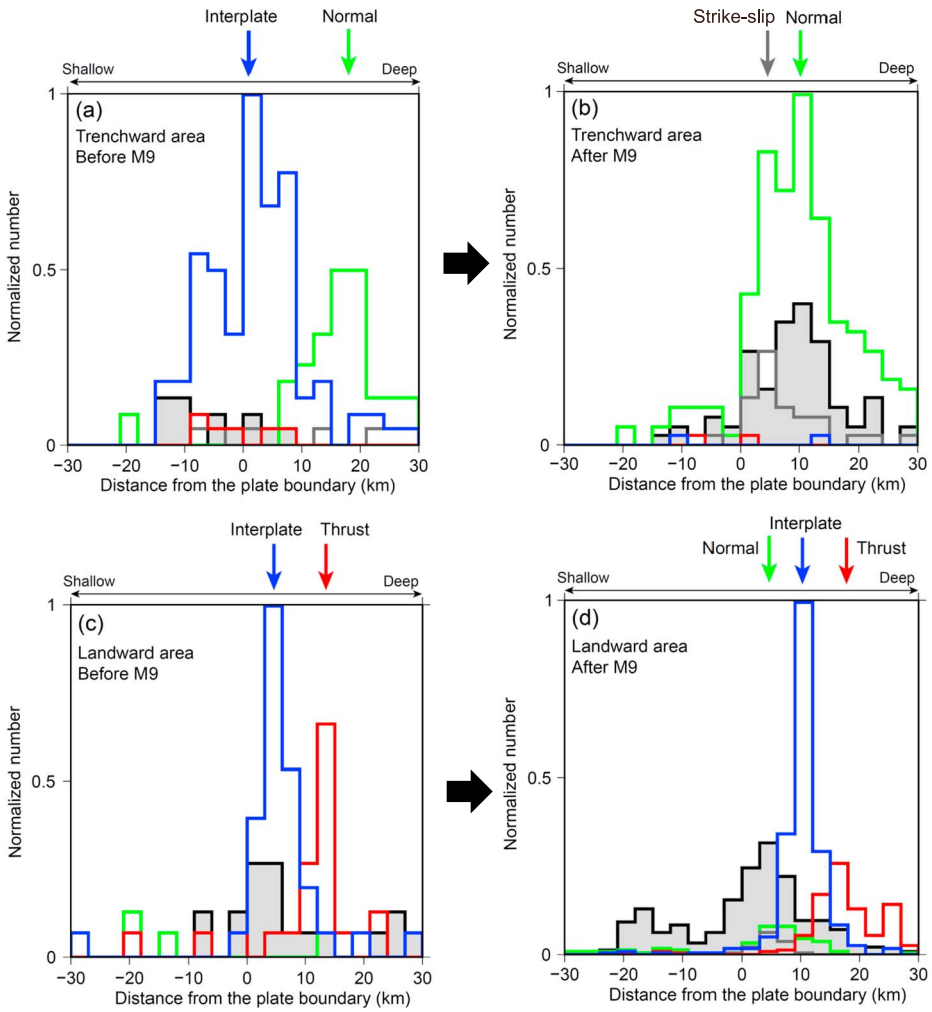

Figure 7. Histogram of earthquakes' depth relative to the plate model [*Nakajima and Hasegawa*, 2006; *Kita et al*., 2010] (gray dashed line in Figures 6c–6f) for (a, b) trenchward and (c, d) landward areas of offshore Miyagi (Figure 6b). The relative depth is calculated for the absolute differences between the event depth and in situ depth of the plate model. The trenchward and landward areas are shown by two rectangles in Figure 6b and are areas where the model plate boundary depth is shallower than 25 km and deeper than 25 km, respectively. Figures 7a and 7c show distributions before the Tohoku-oki earthquake. Figures 7b and 7d show distributions after it. Earthquakes colored gray are other faulting-type events that are not classified as thrust, normal, or strike slip.

faulting earthquakes in the offshore region were relocated at shallower depths than in the original catalogue (Figures 6d and 6f). This is consistent with depth determinations by sP depth phase [*Gamage et al*., 2009] and temporal ocean bottom seismometer (OBS) data analyses for the earthquakes in the area [e.g., *Hino et al*., 2009; *Obana et al*., 2012, 2013; *Yamamoto et al*., 2014]. We also found that most of the normal faulting events (green) in the horizontal range of 0–150 km are located in the upper plate after the Tohoku-oki earthquake (Figures 6d and 6f). Earthquakes classified as interplate types in this study (blue) were relocated under the model plate boundary (dashed line), especially near the Iwate and Miyagi coastline, although there are some outliers (Figures 6c–6f). Therefore, we defined a modified plate boundary based on the relocations performed in this study (thick black line in Figures 6c–6f). Most thrust faulting earthquakes (red) occurred beneath the interplate earthquakes near the coastline (Figure 6f), and the strike-slip faulting earthquakes (gray) seem to be located at or near the area where the normal faulting earthquakes occur (Figure 6f). The region off Iwate Prefecture, which is located outside of the large coseismic slip area of the Tohoku-oki earthquake, is dominated by interplate earthquakes before and after the Tohoku-oki earthquake (Figures 6c and 6d), except for some recent normal faulting events in the horizontal range of 100–150 km (Figure 6d).

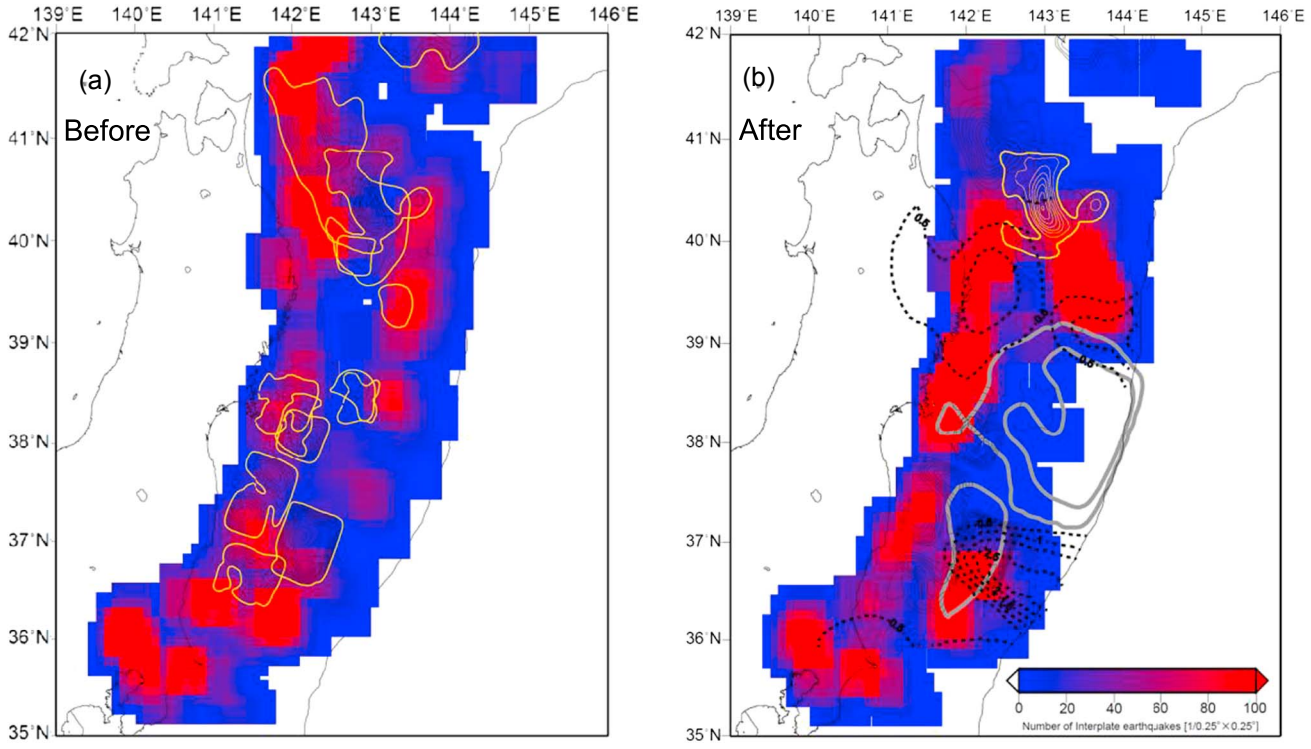

Figure 8. Distribution of the density of interplate earthquakes (a) just before (January 2011 to 11 March 2011, 14:45) and (b) after (11 March 2011, 14:46 to December 2013) the Tohoku-oki earthquake. Yellow contours show the coseismic slip distribution of past $M \geq 7$ interplate earthquakes [*Nagai et al*., 2001; *Yamanaka and Kikuchi*, 2003, 2004; *Murotani*, 2003; *Ohta et al*., 2012]. Gray solid and black dashed lines in Figure 8b are the coseismic slip distribution [*Iinuma et al*., 2012] and postseismic slip distribution [*Sun and Wang*, 2015] of the Tohoku-oki earthquake, respectively.

4.4. Depth Distribution of Faulting Types in and Around the Coseismic Slip Area

Offshore seismicity in subduction zones is sometimes assumed to be interplate earthquakes when there is no available focal mechanism data. However, our results show that 38% of such earthquakes belong to other faulting types. Thrust faulting earthquakes are mostly occurring in the incoming plate (Figures 6d and 6f). Normal faulting earthquakes before the Tohoku-oki earthquake are prominent in the outer trench area. This probably indicates bending stress in the subducting plate. Normal faulting events became prominent in a wider area after the Tohoku-oki earthquake (Figure 5), and they occur in both the upper and lower plates after that event (Figures 6d and 6f). This suggests the strong effect of stress changes due to the large coseismic slip of the Tohoku-oki earthquake as discussed by *Hasegawa et al*. [2011].

To explore the relative location of normal and thrust faulting events, we made histograms of earthquake depth relative to the plate boundary depth for each faulting type for relocated events before and after the Tohoku-oki earthquake (Figure 7). The results show that normal faulting earthquakes in the trenchward region are predominantly in the incoming Pacific plate (plus areas in the distance, deeper than the interplate events) before and after the Tohoku-oki earthquake (Figures 7a and 7b). Note that the interplate earthquakes (blue) are quite widely scattered (±15 km) around the plate boundary depth, probably due to poor depth constraint in this far-offshore area, but still it is clear that the ranges in which normal faulting and interplate events occur are different. In the landward region where the in situ plate boundary depth is about 25 km to 60 km, thrust faulting earthquakes are predominant about 10 km deeper than the peak of the interplate earthquakes before and after the Tohoku-oki earthquake (Figure 7c and 7d). Interestingly, the normal faulting events appeared at shallower depths than the interplate earthquakes after the Tohoku-oki earthquake (Figure 7d), probably due to the change of stress field accompanying the coseismic slip of the Tohoku-oki earthquake. The differences in the peak depth of each of the faulting types relative to the interplate earthquakes, comparing near-shore and far-offshore regions, indicate that there are different dominating stress fields in each area since the Tohoku-oki earthquake.

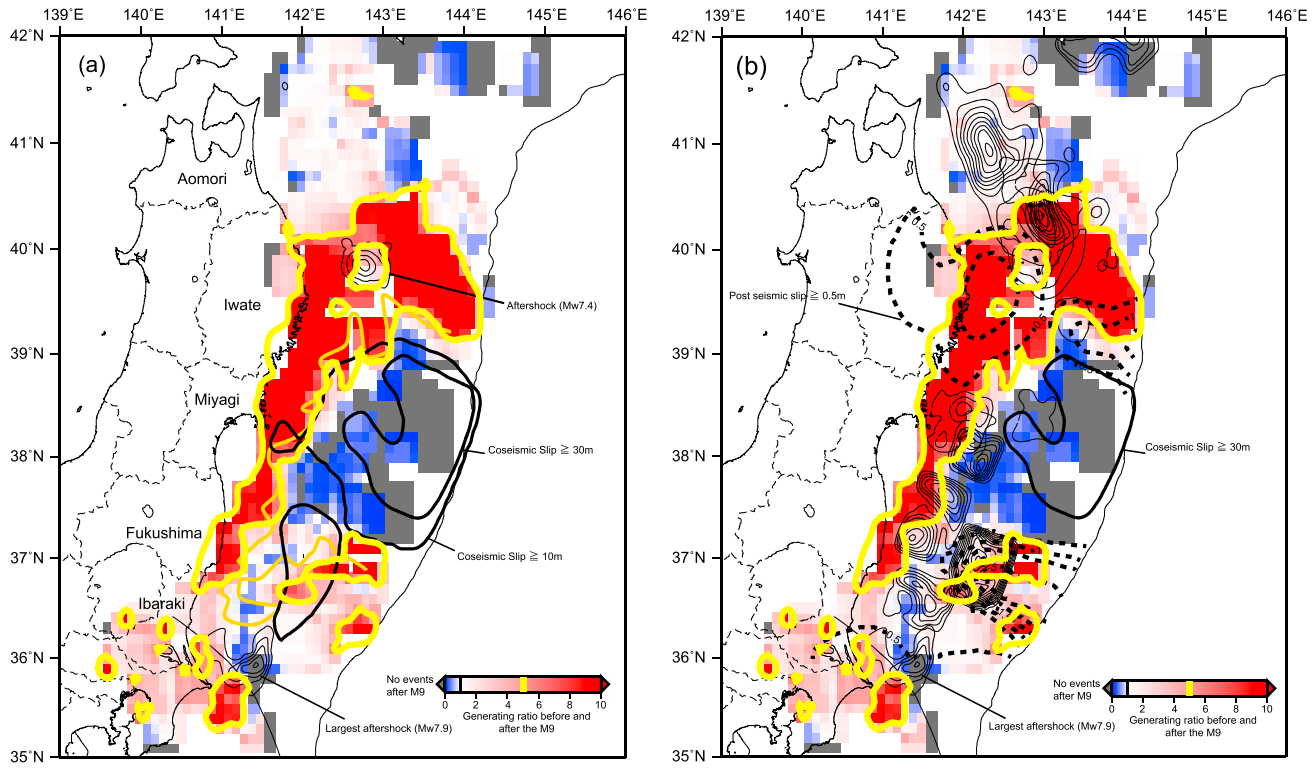

Figure 9. (a) Occurrence ratios of interplate earthquakes after the Tohoku-oki earthquake to that before the earthquake. The black contour is the coseismic slip distribution of the main shock [*Iinuma et al.*, 2012] and its two large interplate aftershocks [*Kubo et al.*, 2013; *Muto et al.*, 2014]. The green line is the outer edge of the coseismic slip area of the Tohoku-oki earthquake [*Kato and Igarashi*, 2012]. The yellow lines are the outer edge of activating area of interplate earthquakes whose occurrence ratio is 5 times higher than that before the Tohoku-oki earthquake. (b) The same as Figure 8a but showing the coseismic slip distributions of $M \geq 7$ interplate earthquakes (black contours) [*Nagai et al.*, 2001; *Yamanaka and Kikuchi*, 2003, 2004; *Murotani*, 2003; *Kubo et al.*, 2013] and the postseismic slip area of the Tohoku-oki earthquake (black dashed line) [*Sun et al.*, 2014].

5. Discussion

5.1. Activities of Interplate Earthquakes Before and After the Tohoku-Oki Earthquake

We examine the distribution of interplate earthquakes before and after the Tohoku-oki earthquake and their relationship with the slip areas of large interplate earthquakes. Figures 8a and 8b show the density of interplate earthquakes along the plate boundary before and after the Tohoku-oki earthquake. The density's pattern is similar for the periods before and after the Tohoku-oki earthquake except for that in the vicinity of the area that underwent coseismic slip during the Tohoku-oki earthquake (Figures 8a and 8b). Areas of low interplate earthquake density (shown in blue) are located in coseismic slip areas of past $M > 7$ earthquakes (yellow contours) [*Nagai et al.*, 2001; *Murotani*, 2003; *Yamanaka and Kikuchi*, 2003, 2004; *Ohta et al.*, 2012] and the Tohoku-oki earthquake (gray contours) [*Iinuma et al.*, 2012], while high-density areas (red colors) are located around the coseismic slip areas. The phenomenon that aftershocks generally occur around the large slip area has been known in previous studies [e.g., *Mendoza and Hartzell*, 1988]; the result in this study shows these observations very clearly. The high-density areas can be interpreted as areas where small- to middle-sized asperities (locked patches) on the plate boundary are dominant and overall interplate locking is relatively small.

To explore the temporal change of interplate seismicity intensity before and after the Tohoku-oki earthquake more precisely, we calculated the ratios of interplate earthquake densities (Figures 9a and 9b) normalized by time (i.e., the ratio of earthquake occurrence rate after the Tohoku-oki earthquake to the rate before). Figures 9a and 9b show the density ratio with coseismic and postseismic slip distributions, respectively. The result shows a clear contrast between areas where interplate earthquakes were highly activated (red) and suppressed (blue). The transition from suppressed areas off Miyagi Prefecture to activated areas probably represents the extent of the coseismic slip. This has been discussed in previous studies using focal

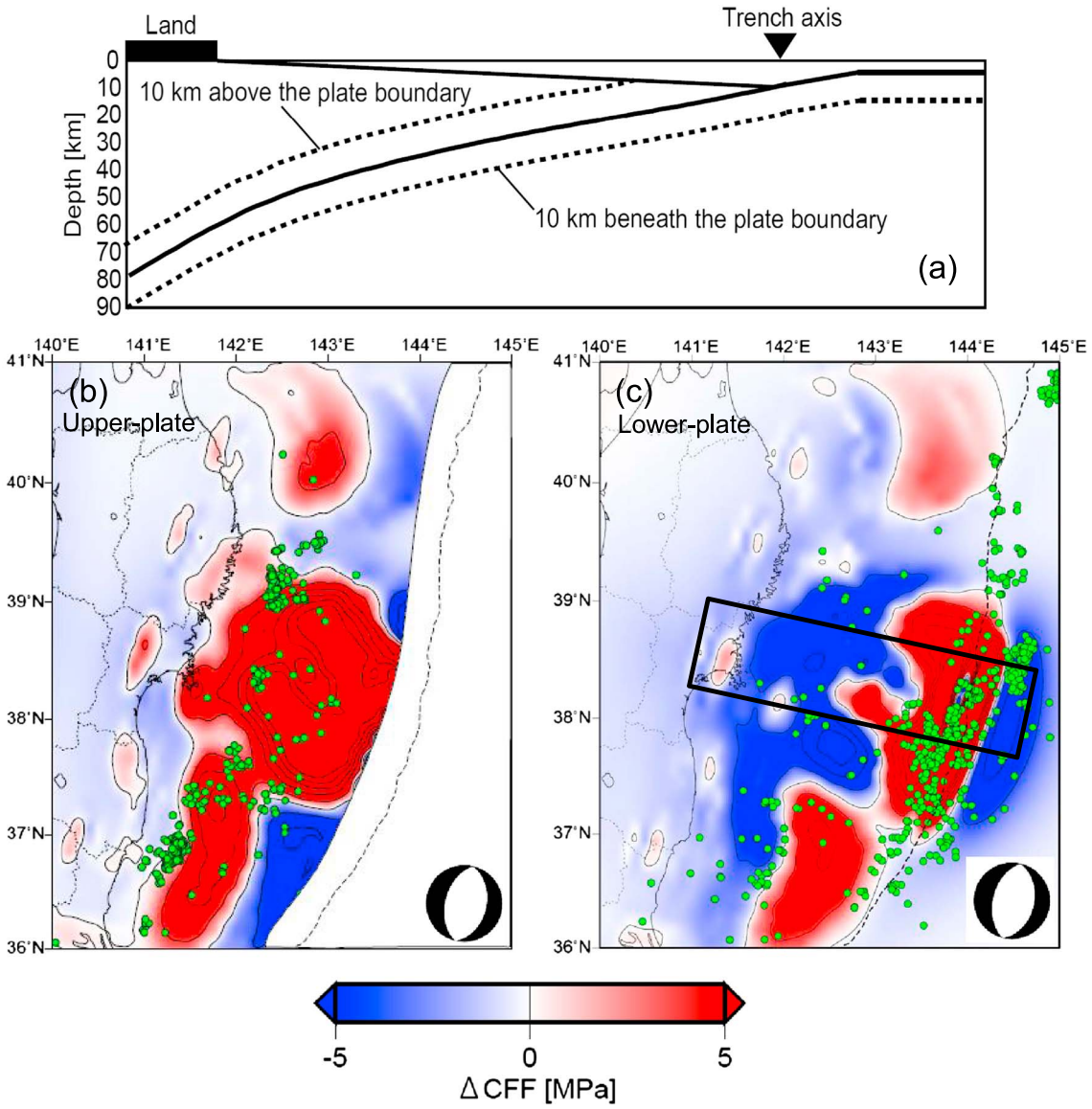

Figure 10. (a) Schematic figure of the location of static stress changes shown in Figures 10b and 10c. (b) Coulomb stress changes for upper plate (above 10 km from the plate boundary) normal faulting earthquakes. The earthquakes 5 to 15 km above the plate boundary were plotted here. (c) Coulomb stress changes for lower plate (below 10 km from the plate boundary) normal faulting earthquakes. The earthquakes 5 to 15 km below the plate boundary were plotted here. The focal mechanism of receiver faults are shown in the bottom right of each figure. Please see main text for details of the receiver faults and assumed constants for calculating Coulomb stress changes. The contour interval in Figures 10b and 10c is 1 MPa.

mechanisms [*Kato and Igarashi*, 2012] (green line in Figure 9a) and seismicity from OBS observations [*Nakatani et al*., 2015]. The narrow suppressed areas (blue) connect the large slip area off Miyagi Prefecture and the largest (*M*7.6) aftershock that occurred 29 min after the Tohoku-oki earthquake [*Kubo et al*., 2013] (black contour). There are also areas where seismicity were highly activated to the southwest of the northeastern edge of the subducted Philippine Sea Plate (yellow line in Figure 9a), suggesting the influence of stress changes due to the *M*9 Tohoku-oki main shock as well as the largest aftershock (contour). Highly activated areas of interplate earthquake also correspond to the area of large postseismic slip of the Tohoku-oki earthquake (black dashed contours in Figure 9b) [*Sun and Wang*, 2015], especially off Iwate Prefecture. Furthermore, the northern limit of the highly activated area corresponds to the southern part of the large coseismic slip of the 1994 Sanriku-oki earthquake (*M*7.6) [*Nagai et al*., 2001] and 1968 Tokachi-oki earthquake (*M*7.9) [*Yamanaka and Kikuchi*, 2004]. This suggests that postseismic slip increases stress on these asperities that probably locked after the earthquakes. In total, these results suggest the following processes on the

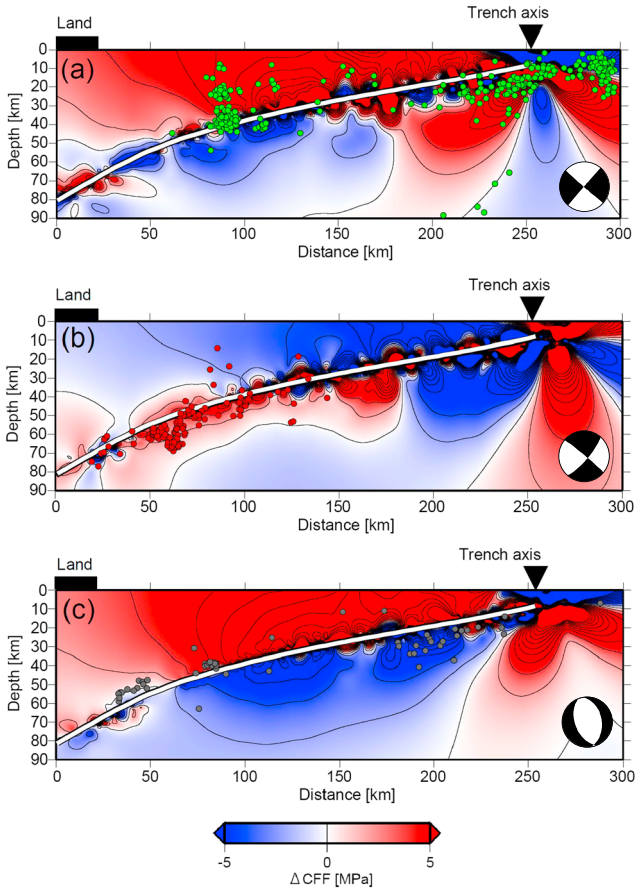

Figure 11. Cross section of Coulomb stress changes for (a) normal faulting, (b) thrust faulting assuming 40° dip, and (c) strike-slip faulting earthquakes offshore Miyagi Prefecture (rectangle area in Figure 10c). Colored circles are the hypocenters of earthquakes within the rectangle area shown in Figure 10c for each receiver faulting type relocated in this study. The focal mechanisms in the figures are for receiver faulting earthquakes viewed in the cross section in Figure 10c. The contour interval is the same as in Figure 10.

plate boundary. (1) In the coseismic slip area, interplate seismicity dramatically decreased, probably due to shear stress release on the plate boundary. (2) Outside of the coseismic slip area off Aomori Prefecture to the Kanto district, interplate seismicity increased, probably due to stress concentrations around the large coseismic slip area and postseismic slip in the area.

It is usually difficult to estimate the spatial extent of offshore coseismic slip with high spatial resolution from onshore geodetic data. The geodetic data easily result in a biased slip distribution due to a trade-off between the distance and slip amount. The activity changes of interplate events are independent data and clearly delineate the spatial extent of coseismic and postseismic slip.

5.2. Aftershock Mechanism Type Distribution and Coulomb Stress Changes Due To the Tohoku-Oki Earthquake

To explore the unique distribution of mechanism types, we examined the relationship between static stress changes due to the Tohoku-oki earthquake and three-dimensional distributions of the earthquake faulting types after that event. We estimated the Coulomb stress changes with an analytical solution of displacement due to faulting in an elastic half space [*Okada*, 1992] using the following parameters: rigidity of 30 GPa, Poisson's ratio of 0.25, and apparent coefficient of friction of 0.4. The input slip model for the Tohoku-oki earthquake's slip [*Iinuma et al.*, 2012] was divided into 10 km × 10 km segments. We set the following typical focal mechanisms as receiver faults: a normal faulting event that occurred in the outer trench region 39 min after the Tohoku-oki earthquake (*M*7.5; latitude, longitude, depth = 144.89, 37.84, 34.0; strike, dip, rake = 194, 49, −89), a thrust faulting event that occurred on 7 April 2011, 23:32 (*M*7.1; latitude, longitude, depth = 141.92, 38.20, 65.7; strike, dip, rake = 20, 40, 81), and a strike-slip faulting event that occurred on 10 July 2011, 09:57; (*M*7.3, latitude, longitude, depth = 143.51, 38.03, 34.0; strike, dip, rake = 64, 84, 16). These receiver mechanisms are plotted in Figures 10 and 11. The Coulomb stress changes for 10 km above and below the plate boundary (Figure 10a) for normal faulting receiver faults indicate that positive static stress change is distributed in a broad area above the coseismic slip area (Figure 10b) and below the coseismic slip area near the Japan Trench (Figure 10c). A nearly opposite-signed stress change can be seen for thrust faulting-type earthquakes in the subducting plate (Figures S2 and S3 in the supporting information). The cross-section for stress change also shows that most normal faulting and thrust faulting events that occurred after the Tohoku-oki earthquake are located in the positive area of static stress change (Figures 11a and 11b). For strike-slip faulting events that occurred after the Tohoku-oki earthquake, however, there is no clear correlation with static stress changes (Figure 11c). This weak correlation could possibly be explained by variation of receiver fault mechanisms, the effects of post seismic slip [e.g., *Ozawa et al.*, 2012] or viscoelastic relaxation [e.g., *Sun et al.*, 2014; *Sun and Wang*, 2015]. Many earthquakes have occurred

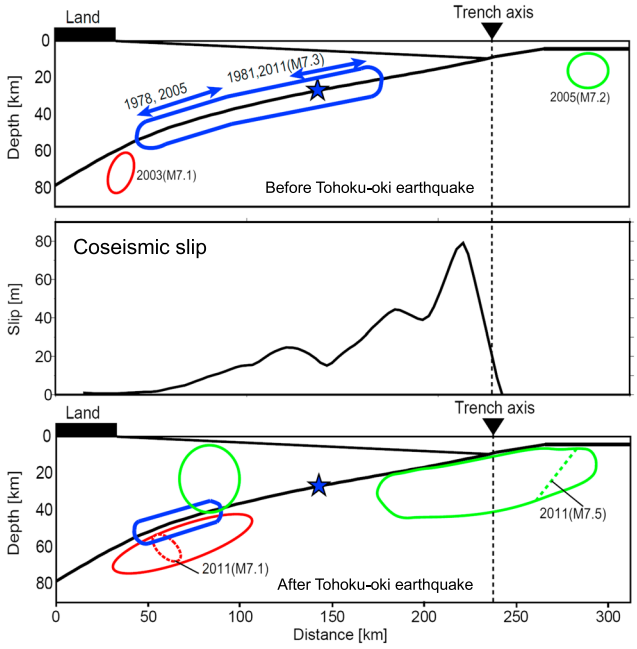

Figure 12. Schematic figure showing earthquake distributions (a) before and (c) after the Tohoku-oki earthquake. Blue, red, and green areas are the locations of interplate, thrust faulting, and normal faulting earthquakes, respectively. The blue star is the hypocenter of the Tohoku-oki earthquake. (b) Trench perpendicular slip distribution of the Tohoku-oki earthquake offshore Miyagi Prefecture (the center of the rectangle in Figure 6b) from the model in *Iinuma et al.* [2012].

long after the main shock, such as the *M*7.1 normal faulting earthquake that occurred on 26 October 2013. To discuss the relationship between the focal mechanisms of aftershocks and stress change in detail, it is necessary to evaluate post-seismic stress changes. Nevertheless, the drastic change in the near-source focal mechanisms before and after the Tohoku-oki earthquake and the good correlation between the stress change and thrust- and normal-faulting earthquakes suggest that the present-day normal and thrust earthquake distribution near the plate boundary is strongly influenced by static stress changes from the Tohoku-oki earthquake, most likely due to low ambient differential stress [*Hasegawa et al.*, 2011; *Hardebeck*, 2012]. The focal mechanism distribution clearly reflects that the stress state around the slip area that probably changed during the great earthquake's cycle.

5.3. Model of the Mechanism Type Distribution and Its Temporal Change

Figure 12 summarizes the distribution of focal mechanism types before and after the Tohoku-oki earthquake across the main slip area. Before the Tohoku-oki earthquake, interplate earthquakes were located in a wide area along the plate boundary, except for the near-trench area (Figure 12, top). This period captured the seismicity just before a great interplate earthquake in its earthquake cycle. It suggests interseismic (or preseismic) slip in the slip zone of the Tohoku-oki earthquake. There was an intermediate amount of coseismic slip in this interseismic slip zone in the Tohoku-oki earthquake as shown in Figure 12 (middle). After the Tohoku-oki earthquake, interplate earthquakes in the large and intermediate coseismic slip areas mostly ceased and prominent seismicity appeared in the upper and lower plates and the plate boundary outside of the slip area (Figure 12, bottom). The first of these two phenomena can be explained by coseismic stress release on the plate boundary as discussed in section 5.1. The second can be explained by intense stress redistribution in the upper and lower plates due to large coseismic slip that occurred in the Tohoku-oki earthquake as discussed in sections 5.2. Nearly complete stress drop in the source area of the Tohoku-oki earthquake is suggested from the dip angle of maximum compressive stress near the plate boundary [*Hasegawa et al.*, 2011]. The widespread normal faulting mechanisms in the subducting plate, not just in the overriding forearc suggest dominance of extensional stress after the Tohoku-oki earthquake. The coseismic changes in focal mechanisms and earthquake distribution before and after the Tohoku-oki earthquake suggest that the mechanism type and distribution around the source area of a megathrust earthquake is not steady during its earthquake cycle.

6. Conclusion

We found that there is a good correlation between the degree of similarity of focal mechanisms and waveforms of earthquake pairs in the NE Japan subduction zone. Using this relationship, we classified the faulting types of earthquakes whose focal mechanisms were unknown into interplate, thrust, normal, and strike-slip events. The results show that interplate earthquakes dominate in the study region (62%), but there are considerable numbers of earthquakes with other faulting types. This is an important observation when discussing offshore seismicity. The 8984 events that were newly classified in this study doubles the number of events with known

mechanism types in this area. The spatial distribution of mechanism types revealed the following characteristics. (1) Interplate earthquakes are distributed in a complementary fashion with the main coseismic slip areas of $M > 7$ interplate earthquakes. (2) After the 2011 Tohoku-oki earthquake, very few interplate earthquakes occurred in areas where it produced middle to large coseismic slip up through the end of 2013. (3) The activation of interplate earthquakes around the coseismic slip area show the spatial extent of postseismic slip that may cause major additional interplate aftershocks in the asperities of historical earthquakes. (4) Taking into account the position of hypocenters relocated using a double-difference method with a 3-D velocity structure, the spatial distributions of focal mechanisms near the Tohoku-oki earthquake after the earthquake are well explained by the static stress changes accompanying the Tohoku-oki earthquake.

In total, the focal mechanism types from the template search and earthquake relocation characterized present seismicity and interplate coupling condition that changed dramatically in the area offshore Tohoku when the 2011 Tohoku-oki earthquake occurred, producing heterogeneous stress distribution around its source.

Acknowledgments

We are grateful to Editor Paul Tregoning and two anonymous reviewers for helpful comments that improved our article very much. We thank the Japan Meteorological Agency (JMA) for use of its earthquake catalogue and phase data, the National Research Institute for Earth Science and Disaster Prevention (NIED) for its focal mechanisms catalogue, Hokkaido University, Hirosaki University, Tohoku University, and the University of Tokyo for their seismic waveform data. The earthquake catalogue and phase data used in this study are available at http://www.jma.go.jp subject to the policies of JMA. The focal mechanism data used in this study are available at http://www.bosai.go.jp subject to the policies of NIED. The waveform data are available at http://wwweic.eri.u-tokyo.ac.jp/harvest/ subject to the policies of Hokkaido University, Hirosaki University, Tohoku University, and the University of Tokyo. We also thank T. Iinuma and Y. Ohta for data on the coseismic slip distribution of the 2011 Tohoku-oki earthquake and the *M*7.3 foreshock, respectively, A. Hasegawa, R. Hino, T. Shiina, Y. Suzuki, and N. Hatakeyama of Tohoku University; J. Nakajima, of Tokyo Institute of Technology; S. Kita of Hiroshima University; T. Hashimoto of the Japan Meteorological Agency; and R. Bürgmann of the University of California, Berkeley for their fruitful discussions. Some figures were drawn using the Generic Mapping Tools software [*Wessel and Smith*, 1998].

References

Abers, G. A., and J. W. Gephart (2001), Direct inversion of earthquake first motions for both the stress tensor and focal mechanisms and application to Southern California, *J. Geophys. Res.*, *106*, 26,523–26,540, doi:10.1029/2001JB000437.

Asano, Y., T. Saito, Y. Ito, K. Shiomi, H. Hirose, T. Matsumoto, S. Aoi, S. Hori, and S. Sekiguchi (2011), Spatial distribution and focal mechanisms of aftershocks of the 2011 off the Pacific coast of Tohoku Earthquake, *Earth Planet. Space.*, *63*, 669–673.

Dreger, D., and D. V. Helmberger (1993), Determination of source parameters at regional distances with three-component sparse network data, *J. Geophys. Res.*, *98*, 8107–8125, doi:10.1029/93JB00023.

Ellsworth, W. L. (1995), Characteristic earthquake and long-term earthquake forecasts: Implications of central California seismicity, in *Urban Disaster Mitigation: The Role of Science and Technology*, edited by F. Y. Cheng and M. S. Sheu, Elsevier, Oxford, U. K.

Frohlich, C. (1992), Triangle diagrams: Ternary graphs to display similarity and diversity of earthquake focal mechanism, *Phys. Earth Planet. Inter.*, *75*, 193–198.

Fukuyama, E., Ishida, M., Dreger, D. S., Kawai, H. (1998), Automated seismic moment tensor determination by using on-line broadband seismic waveforms. *Zisin*, 149–156 (in Japanese with English abstract).

Gamage, S. S. N., N. Umino, A. Hasegawa, and S. H. Kirby (2009), Offshore double-planed shallow seismic zone in the NE Japan forearc region revealed by sP depth phases recorded by regional networks, *Geophys. J. Int.*, *178*, 195–214, doi:10.1111/j.1365-246X.2009.04048.x.

Harada, T., S. Murotani, and K. Satake (2013), A deep outer-rise reverse-fault earthquake immediately triggered a shallow normal-fault earthquake: The 7 December 2012 off-Sanriku earthquake (M_W 7.3), *Geophys. Res. Lett.*, *40*, 4214–4219, doi:10.1002/grl.50808.

Hardebeck, J. (2012), Coseismic and postseismic stress rotations due to great subduction zone earthquakes, *Geophys. Res. Lett.*, *39*, L21313, doi:10.1029/2012GL053438.

Hasegawa, A., N. Umino, and A. Takagi (1978), Double-planed structure of the deep seismic zone in the northeastern Japan arc, *Tectonophysics*, *47*, 43–58.

Hasegawa, A., K. Yoshida, and T. Okada (2011), Nearly complete stress drop in the 2011 *Mw* 9.0 off the Pacific coast of Tohoku Earthquake, *Earth Planets Space*, *63*, 703–707.

Hino, R., S. Ito, H. Shiobara, H. Shimamura, T. Sato, T. Kanazawa, and A. Hasegawa (2000), Aftershock distribution of the 1994 Sanriku-oki earthquake (*Mw*7.7) revealed by ocean bottom seismographic observation, *J. Geophys. Res.*, *105*, 21,697–21,710, doi:10.1029/2000JB900174.

Hino, R., R. Azuma, Y. Ito, Y. Yamamoto, K. Suzuki, H. Tsushima, S. Suzuki, M. Miyashita, M. A. Tomori, and G. Tange (2009), Insight into complex rupturing of the aftershocks of the 2005 Sanriku earthquake (*Mw* = 7.0) located by ocean bottom seismometry, *Geochem. Geophys. Geosyst.*, *10*, Q07O18, doi:10.1029/2009GC002415.

Ide, S., A. Baltay, and G. C. Beroza (2011), Shallow dynamic overshoot and energetic deep rupture in the 2011 *Mw* 9.0 Tohoku-oki earthquake, *Science*, *332*, 1427–1429.

Igarashi, T., T. Matsuzawa, N. Umino, and A. Hasegawa (2001), Spatial distribution of focal mechanisms for interplate and intraplate earthquakes associated with the subducting Pacific plate beneath the northeastern Japan arc: A triple-planed deep seismic zone, *J. Geophys. Res.*, *106*(B2), 2177–2191, doi:10.1029/2000JB900386.

Iinuma, T., et al. (2012), Coseismic slip distribution of the 2011 off the Pacific Coast of Tohoku Earthquake (*M*9.0) refined by means of seafloor geodetic data, *J. Geophys. Res.*, *117*, B07409, doi:10.1029/2012JB009186.

Ito, Y., H. Matsubayashi, H. Kimura, T. Matsumoto, Y. Asano, and S. Sekiguchi (2004), Spatial distribution for moment tensor solutions of the 2003 Tokachi-oki earthquake (MJMA = 8.0) and aftershocks, *Earth Planets Space*, *56*, 301–306.

Kagan, Y. Y. (1991), 3-D rotation of double-couple earthquake sources, *Geophys. J. Int.*, *106*, 709–716.

Kato, A., and S. Nakagawa (2014), Multiple slow-slip events during a foreshock sequence of the 2014 Iquique, Chile *Mw* 8.1 earthquake, *Geophys. Res. Lett.*, *41*, 5420–5427, doi:10.1002/2014GL061138.

Kato, A., and T. Igarashi (2012), Regional extent of the large coseismic slip zone of the 2011 *Mw* 9.0 Tohoku-Oki earthquake delineated by on-fault aftershocks, *Geophys. Res. Lett.*, *39*, L15301, doi:10.1029/2012GL052220.

Kato, A., K. Obara, T. Igarashi, H. Tsuruoka, S. Nakagawa, and N. Hirata (2012), Propagation of slow slip leading up to the 2011 *Mw*9.0 Tohoku-Oki earthquake, *Science*, *335*, doi:10.1126/science.1215141.

Kita, S., T. Okada, A. Hasegawa, J. Nakajima, and T. Matsuzawa (2010), Existence of interplane earthquakes and neutral stress boundary between the upper and lower planes of the double seismic zone beneath Tohoku and Hokkaido, northeastern Japan, *Tectonophysics*, *496*, 68–82.

Kubo, H., K. Aasano, and T. Iwata (2013), Source-rupture process of the 2011 Ibaraki-oki, Japan, earthquake (*Mw*7.9) estimated from the joint inversion of strong-motion and GPS Data: Relationship with seamount and Philippine Sea Plate, *Geophys. Res. Lett.*, *40*, 3002–3007, doi:10.1002/grl.50558.

Lay, T., Z. Duputel, L. Ye, and H. Kanamori (2013), The December 7, 2012 Japan Trench intraplate doublet (*Mw* 7.2, 7.1) and interactions between near-trench intraplate thrust and normal faulting, *Phys. Earth Planet. Inter.*, *220*, 73–78, doi.10.1016/j.pepi.2013.04.009.

Loveless, J. P., and B. J. Meade (2010), Geodetic imaging of plate motions, slip rates, and partitioning of deformation in Japan, *J. Geophys. Res.*, *115*, B02410, doi:10.1029/2008JB006248.
Mendoza, C., and S. H. Hartzell (1988), Aftershock patterns and main shock faulting, *Bull. Seismol. Soc. Am.*, *78*(4), 1438–1449.
Menke, W. (1999), Using waveform similarity to constrain earthquake locations, *Bull. Seismol. Soc. Am.*, *89*, 1143–1146.
Menke, W., A. L. Lerner-Lam, B. Dubendorff, and J. Pacheco (1990), Polarization and coherence of 5 to 30 Hz seismic wave fields at a hard-rock site and their relevance to velocity heterogeneities in the crust, *Bull Seismol. Soc. Am.*, *80*, 430–449.
Murotani, S. (2003), Rupture processes of large Fukushima-Oki earthquakes in 1938, MSc thesis, Univ. of Tokyo, Tokyo.
Muto, D., H. Ueno, Y. Kawazoe, and K. Iwakiri (2014), The analysis of the source processes of the foreshocks and aftershocks of the 2011 off the Pacific coast of Tohoku earthquake [in Japanese], *Q. J. Seismol.*, *78*, 29–44.
Nagai, R., M. Kikuchi, and Y. Yamanaka (2001), Comparative study on the source processes of recurrent large earthquakes in Sanriku-oki Region: The 1968 Tokachi-oki earthquake and the 1994 Sanriku-oki earthquake, *Zisin(2)*, *54*, 267–280.
Nakahara, H. (2004), Correlation distance of waveforms for closely located events: 1. Implication of the heterogeneous structure around the source region of the 1995 Hyogo-Ken Nanbu, Japan, earthquake (*Mw* = 6.9), *Geophys. J. Int.*, *157*, 1255–1268, doi:10.1111/j.1365-236X.2004.02278.x.
Nakajima, J., and A. Hasegawa (2006), Anomalous low-velocity zone and linear alignment of seismicity along it in the subducted Pacific slab beneath Kanto, Japan: Reactivation of subducted fracture zone?, *Geophys. Res. Lett.*, *33*, L16309, doi:10.1029/2006GL026773.
Nakajima, T. (1974), Spatial and sequential distribution of focal mechanisms before and after the Tokachi-oki earthquake of May 16, 1968, *Geophys. Bull. Hokkaido Univ.*, *32*, 25–42.
Nakatani, Y., K. Mochizuki, M. Shinohara, T. Yamada, R. Hino, Y. Ito, Y. Murai, and T. Sato (2015), Changes in seismicity before and after the 2011 Tohoku earthquake around its southern limit revealed by dense ocean bottom seismic array data, *Geophys. Res. Lett.*, *42*, 1384–1389, doi:10.1002/2015GL063140.
Obana, K., G. Fujie, T. Takahashi, Y. Yamamoto, Y. Nakamura, S. Kodaira, N. Takahashi, Y. Kaneda, and M. Shinohara (2012), Normal-faulting earthquakes beneath the outer slope of the Japan Trench after the 2011 Tohoku earthquake: Implications for the stress regime in the incoming Pacific plate, *Geophys. Res. Lett.*, *39*, L00G24, doi:10.1029/2011GL050399.
Obana, K., et al. (2013), Aftershocks near the updip end of the 2011 Tohoku-oki earthquake, *Earth Planet. Sci. Lett.*, *382*, 111–116, doi:10.1016/j.epsl.2013.09.007.
Ohta, Y., et al. (2012), Geodetic constraints on afterslip characteristics following the March 9, 2011, Sanriku-oki earthquake, Japan, *Geophys. Res. Lett.*, *39*, L16304, doi:10.1029/2012GL052430.
Okada, T., K. Yoshida, S. Ueki, J. Nakajima, N. Uchida, T. Matsuzawa, N. Umino, A. Hasegawa, and Group for the aftershock observations of the 2011 off the Pacific coast of Tohoku earthquake (2011), Shallow inland earthquakes in NE Japan possibly triggered by the 2011 off the Pacific coast of Tohoku earthquake, *Earth Planets Space*, *63*(7), 749–754, doi:10.5047/eps.2011.06.027.
Okada, Y. (1992), Internal deformation due to shear and tensile faults in a half space, *Bull. Seismol. Soc. Am.*, *82*, 1018–1040.
Ozawa, S., T. Nishimura, H. Munekane, H. Suito, T. Kobayashi, M. Tobita, and T. Imakiire (2012), Preceding, coseismic, and postseismic slips of the 2011 Tohoku earthquake, Japan, *J. Geophys. Res.*, *117*, B07404, doi:10.1029/2011JB009120.
Peng, Z., and P. Zhao (2009), Migration of early aftershocks following the 2004 Parkfield earthquake, *Nat. Geosci.*, doi:10.1038/NGO697.
Poupinet, G., W. L. Ellsworth, and J. Frechet (1984), Monitoring velocity variations in the crust using earthquake doublets: An application to the Calaveras fault, California, *J. Geophys. Res.*, *89*(B7), 5719–5731, doi:10.1029/JB089iB07p05719.
Satake, K., Y. Fujii, T. Harada, and Y. Namegaya (2013), Time and slip distribution of coseismic slip of the 2011 Tohoku earthquake as inferred from tsunami waveform data, *Bull. Seismol. Soc. Am.*, *102*(2B), 1473–1492, doi:10.1785/0120120122.
Sella, G. F., T. H. Dixon, and A. Mao (2002), REVEL: A model for Recent plate velocities from space geodesy, *J. Geophys. Res.*, *107*(B4), doi:10.1029/2000JB000033.
Shiina, T., J. Nakajima, and T. Matsuzawa (2013), Seismic evidence for high pore pressure in the oceanic crust: Implications for fluid-related embrittlement, *Geophys. Res. Lett.*, *40*, 2006–2010, doi:10.1002/grl.50468.
Sun, T., and K. Wang (2015), Viscoelastic relaxation following subduction earthquakes and its effects on afterslip determination, *J. Geophys. Res. Solid Earth*, *120*, 1329–1344, doi:10.1002/2014JB011707.
Sun, T., et al. (2014), Prevalence of viscoelastic relaxation after the 2011 Tohoku-oki earthquake, *Nature*, *514*, 84–87, doi:10.1038/nature13778.
Suwa, Y., S. Miura, A. Hasegawa, T. Sato, and K. Tachibana (2006), Interplate coupling beneath NE Japan inferred from three-dimensional displacement field, *J. Geophys. Res.*, *111*, B04402, doi:10.1029/2004JB003203.
Toda, S., J. Lin, and S. Stein (2011), Using the 2011 *Mw*9.0 off the Pacific coast of Tohoku earthquake to test the Coulomb stress triggering hypothesis and to calculate faults brought closer to failure, *Earth Planets Space*, *63*, 725–730.
Uchida, N., and T. Matsuzawa (2013), Pre- and postseismic slow slip surrounding the 2011 Tohoku-oki earthquake rupture, *Earth Planet. Sci. Lett.*, *374*, 81–91.
Uchida, N., J. Nakajima, A. Hasegawa, and T. Matsuzawa (2009), What controls interplate coupling? Evidence for abrupt change in coupling across a border between two overlying plates in the NE Japan subduction zone, *Earth Planet. Sci. Lett.*, *283*, 111–121.
Uchida, N., T. Matsuzawa, J. Nakajima, and A. Hasegawa (2010), Subduction of a wedge-shaped Philippine Sea Plate beneath Kanto, central Japan, estimated from converted waves and small repeating earthquakes, *J. Geophys. Res.*, *115*, B07309, doi:10.1029/2009JB006962.
Wessel, P., and W. H. Smith (1998), New, improved version of the Generic Mapping Tools released, *Eos Trans. AGU*, *79*, 579, doi:10.1029/98EO00426.
Yamamoto, Y., K. Obana, S. Kodaira, R. Hino, and M. Shinohara (2014), Structural heterogeneities around the megathrust zone of the 2011 Tohoku earthquake from tomographic inversion of onshore and offshore seismic observations, *J. Geophys. Res. Solid Earth*, *119*, 1165–1180, doi:10.1002/2013JB010582.
Yamanaka, Y., and M. Kikuchi (2003), Source process of the recurrent Tokachi-oki earthquake on September 26, 2003, inferred from teleseismic body waves, *Earth Planets Space*, *55*, e21–e24.
Yamanaka, Y., and M. Kikuchi (2004), Asperity map along the subduction zone in northeastern Japan inferred from regional seismic data, *J. Geophys. Res.*, *109*, B07307, doi:10.1029/2003JB002683.
Zhang, H., and C. H. Thurber (2003), Double-difference tomography: The method and its application to the Hayward fault, California, *Bull. Seismol. Soc. Am.*, *93*, 1875–1889.
Zhang, H., and C. H. Thurber (2006), Development and applications of double-differene seismic tomography, *Pure Appl. Geophys.*, *163*, 373–403.